Available online at www.sciencedirect.com

SciVerse ScienceDirect

Ceramics International 38 (2012) 6171–6179

CERAMICS INTERNATIONAL

www.elsevier.com/locate/ceramint

Studies on the resistive response of nickel and cerium doped SnO_2 thick films to acetone vapor

L.K. Bagal[a], J.Y. Patil[a], I.S. Mulla[b,c], S.S. Suryavanshi[a,*]

[a]*School of Physical Sciences, Solapur University, Solapur 413255, India*
[b]*National Chemical Laboratory, Pune 411008, India*
[c]*Emeritus Scientist, Centre for Materials for Electronic Technology (C-MET), Pune 411008, India*

Received 20 March 2012; received in revised form 18 April 2012; accepted 20 April 2012
Available online 5 May 2012

Abstract

Undoped and Ni, Ce-doped nanocrystalline tin oxide were synthesized by co-precipitation route. Doped as well as undoped SnO_2 compositions revealed single phase structure without any impurity. The lattice constant of SnO_2 increases and the grain size decreases with doping of Ni and Ce. The responses of the sensing elements are evaluated by measuring the resistance change upon exposure to various test gases such as liquid petroleum gas (LPG), acetone, ethanol and ammonia. In comparison to LPG, ethanol, and ammonia the response towards acetone vapor increases markedly on simultaneous doping of Ni and Ce. For acetone vapors with 500 ppm at 300 °C, the undoped SnO_2 shows 31% response, while with individual Ni or Ce doping it increases to 38 and 60%, respectively, however with simultaneous doping of Ni and Ce there is a significant enhancement up to 92%. The results of gas sensing measurements reveal that the thick films deposited on alumina substrates using screen printing technique give selectively a high response of (87%) with fast recovery (~1 min) towards 100 ppm acetone at 300 °C.

Keywords: SnO_2; Screen-printing; Acetone vapor; (Ni+Ce)-doping

1. Introduction

Gas sensors have numerous applications in industries, environment monitoring and protection. Acetone is generally used as chemical reagent in industry and it easily evaporates at room temperature. Human being may develop headache, fatigue if the concentration of acetone in air is higher than 10,000 ppm. The medical reports specify that the diabetic patients possess high acetone in their blood and saliva [1,2] and hence they exhale high acetone. Therefore detection and measurement of acetone concentration in the work place of human body is quite essential for our safety and health. Several analytical techniques are available to measure the concentration of acetone such as chromatographic analysis, spectroscopy and sensors [2–5]. Among these, detection by the sensor is the most prominent method due to its simplicity, convenience and reliability. Of all the known metal oxides used as sensors, tin oxide is the prominent and widely used metal oxide gas sensors due to its capability to detect various toxic, hazardous and flammable gases with high response, selectivity and good stability. SnO_2 sensors are generally operated at high temperatures which limit their applications for detecting combustible gases. In order to improve the gas sensing properties like rate of response, time and selectivity to a single gas, noble metals are used as additives, which would perhaps act as catalyst and lower the operating temperature [6–10]. The effect of doping of Cu [11], Ni [12], Ni+Al [12] and Co [13] have been reported by various authors and has been found to exhibit gas sensing behavior towards both oxidizing and reducing gases, which is correlated to decrease in grain size and depleted space charge layer. The additives like ZnO, CuO, MnO, etc. have been reported to enhance densification when samples are fired at temperature greater than 800 °C [14–16]. However such densified samples are not porous and hence they do not exhibit good response. The doping

*Corresponding author. Tel.: +91 217 2744771; fax: +91 217 2744770.
E-mail address: sssuryavanshi@rediffmail.com (S.S. Suryavanshi).

0272-8842/$36.00
http://dx.doi.org/10.1016/j.ceramint.2012.04.068

of nickel, copper in tin oxide gas sensor has been studied by various researchers, and they have concluded that doping of NiO or CuO inhibit the grain growth, as a result small segregated grains of Ni, Cu appear on the surface of SnO_2 [17,18]. However, in general, the simultaneously Ni and Ce doped SnO_2 as acetone sensor is not reported and a lot of work can be done to realize their sensing mechanism. In the present work the gas sensing behavior of undoped, nickel, cerium and nickel with cerium doped SnO_2 synthesized by using co-precipitation method is studied.

2. Experimental

2.1. Preparation of undoped and doped SnO_2 powder

SnO_2 powder was prepared by a simple co-precipitation route. All the chemicals used in this work are of AR grade. In a typical experiment, an appropriate quantity of stannic chloride ($SnCl_4 \cdot 5H_2O$) and ammonia solution (NH_4OH 25%) were used as precursors. The stannic chloride was dissolved in distilled water to form 0.1 M transparent solution. Dilute ammonia was added drop-wise in the solution under magnetic stirring until pH of the solution becomes 8–9 at which precipitation of functional material occurs. The resulting precipitate was then filtered and washed with distilled water for several times to remove chloride ions [19]. The resulting product was kept for drying under IR lamp for about 8 h, which was followed by calcinations in air at 450 °C for 2 h. This sample was labeled as S1.

The 98 wt% stannic chloride and 2 wt% $NiSO_4$ were added together in water to form a transparent solution with desired concentration. Dilute ammonia was added to the solution to precipitate the constituents together. The precipitates were filtered and washed using distilled water and further the procedure was adopted as in S1, and the resulting sample was labeled as S2.

The 96 wt% stannic chloride and 4 wt% $Ce(NO_3)_3$ were added together in water to form a transparent solution with desired concentration. Dilute ammonia was added slowly to precipitate and further procedure was adopted as per S1, and the resulting sample was labeled as S3.

The 94 wt% stannic chloride, 4 wt% $Ce(NO_3)_3$ and 2 wt% $NiSO_4$ were added together in water to form a transparent solution with desired concentration. Dilute ammonia was added slowly to precipitate and further procedure was adopted as per S1. The resulting sample was labeled as S4. Table 1 shows the sample preparation details.

2.2. Sensor experiment

The calcinated powder of functional material was mixed thoroughly with 8% bismuth oxide as inorganic binder, 8% ethyl cellulose as organic vehicle and butyl carbitol acetate to achieve proper thixotropic properties of the paste. They were used in weight ratio of 100:8:8 to achieve adhesiveness. This thixotropic paste was further used to deposit thick films on ultrasonically cleaned alumina substrate (10×20 mm^2) by using screen printing technique with the nylon cloth of 140 mesh counts. The details of the technique are described elsewhere [20,21]. The resulting thick films were sintered in air at 650 °C for 2 h in muffle furnace.

Table 1
Sample identification for SnO_2.

Sample code	Composition
S1	Undoped SnO_2 using coprecipitation method
S2	98 wt% $SnCl_4$+2 wt% $NiSO_4$
S3	96 wt% $SnCl_4$+4 wt% $Ce(NO_3)_3$
S4	94 wt% $SnCl_4$+2 wt% $NiSO_4$+4 wt% $Ce(NO_3)_3$

Ohmic contacts were provided by using conducting silver paste on thick film. These thick films were subjected for studying their gas sensing properties towards the known amount of various test gases using the dynamic gas sensing set-up shown elsewhere [22]. The sensor was kept in the same experimental chamber in air as medium and relative humidity (RH) was about 40%. The known amount of test gas was introduced in the gas-mixing chamber so that their required part per million (ppm) concentrations is attained. The gas-sensing characteristics with reference to test gas, operating temperature and concentration of test gas were recorded using Digital Nanoammeter Model DNM-121 and ScienTECH variable power supply ST4074. The gas sensing characteristics of all the samples were investigated towards four different gases (LPG, acetone, ethanol and ammonia) under identical experimental conditions. The resistance of the sample in presence of air and in presence of test gas was measured. The experiment was repeated twice to check the repeatability of the sensor. The gas response was defined as $S=(R_a-R_g)/R_a$, where, R_a is resistance of sensor in air and R_g is resistance in presence of test gas.

3. Results and discussion

3.1. Characterization of the sensors

The crystal structure of the synthesized nanopowders was investigated with X-ray diffractometer (BRUKER AXS D8-Advanced) with Cu Kα line at 1.542 Å. Fig. 1 shows the XRD patterns of sintered samples S1, S2, S3, and S4. All the diffraction peaks have been indexed to the tetragonal rutile structure of SnO_2 with lattice constants which are in good agreement with the reported values ($a=4.750$ Å and $c=3.196$ Å) from JCPDS card (No. 77-0451). For Ni, Ce-doped SnO_2 no diffraction peaks of Ni, Ce oxides or other impurity phases were observed, suggesting that Ni^{2+}, Ce^{3+} ions get uniformly substituted into the Sn^{4+} sites or interstitial sites in SnO_2 lattice. Moreover, the major diffraction peaks shift slightly

towards smaller diffraction angle compared to the standard card. The increase in lattice parameter with incorporation of Ni, Ce and Ni+Ce is attributed to the large ionic radii [23] of Ni^{2+} (69 pm), Ce^{3+} (115 pm) which substitute the smaller Sn^{4+} (69 pm) ion. In addition, the reduction in peak intensity and the width broadening on doping of Ni^{2+}, Ce^{3+} and Ni^{2+} with Ce^{3+} in the SnO_2 nanoparticles facilitates formation of smaller average diameter crystallites. The crystallite size determined from the Scherrer equation for various sintered compositions of SnO_2 are presented in Table 2, which indicates that the crystallite size decreases with doping. The doping of nickel and cerium reduces the crystallite size of SnO_2 and these results are in good agreement with earlier reports [24,25]. Moreover with doping of nickel and cerium, the crystallinity reduces significantly which is also evidenced from the SAED studies [26].

The surface morphology of all the compositions was studied using a scanning electron microscope (Instrument JSM-6360). Fig. 2 depicts the SEM images of sintered thick films of all the samples. The microstructure reveals formation of the agglomerated grains having size < 1 μm with remarkable porosity which facilitates gas response.

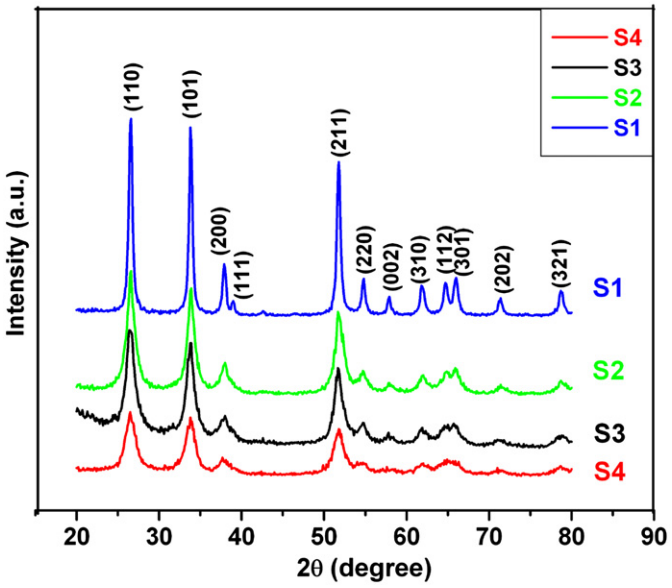

Fig. 1. XRD patterns of undoped (S1), Ni-doped (S2), Ce-doped (S3) and (Ni+Ce)-doped SnO_2 (S4).

Table 2
Average particle size and lattice parameters of undoped, Ni-doped, Ce-doped and (Ni+Ce)-doped SnO_2.

Sample	Average particle size (nm) from XRD	Average particle size (nm) from TEM	Lattice parameter	
			a (Å)	*c* (Å)
S1	16	17	4.738	3.165
S2	9	9	4.761	3.185
S3	8	8	4.768	3.188
S4	6	7	4.771	3.197

The high surface area available for the adsorption of test gas plays an important role in gas response [27]. The elemental composition obtained from the EDAX spectrum (Fig. 3) confirms the presence of Ni, Ce, Sn and oxygen. Table 3 shows that the EDAX data is in good agreement with the initial precursor concentration.

The shape and size of the nanostructures are determined by TEM. The TEM analysis was carried out using PHILIPS (Model-CM200) operated at 200 kV with resolution of 0.24 nm. A typical TEM image (Fig. 4(a)) of the undoped SnO_2 sintered at 650 °C, shows formation of nanoparticles uniformly distributed with about 17 nm size. The TEM image of the Ni-doped SnO_2 (Fig. 4(b)) shows nearly cubical shaped discrete nanoparticles of < 10 nm size. The diffraction rings corresponding to (101), (111), (220), (310), and (202) planes are clearly seen in SAED pattern which also matches with XRD planes. The TEM image (Fig. 4(c)) of Ce-doped SnO_2 nanoparticles reveal that the doped materials present small particles with sizes about 8 nm. The TEM image (Fig. 4(d)) of the Ni with Ce-doped SnO_2 shows formation of nanoparticles uniformly distributed having nearly hexagonal shape. The diameter of the particles varies from 4–8 nm with majority of the particles having 7 nm diameter showing clear boundaries. The Selected Area Electron Diffraction (SAED) pattern (shown in inset) of an isolated particle shows bright rings corresponding to the (200), (002), (112), (202) lattice planes of SnO_2 structure. These lattice planes match well with the planes observed in the XRD pattern. It is observed that on doping of Ni along with Ce, the particle size is decreased and hence high gas response is exhibited (Sample S4). The average particle size of all the samples obtained from TEM images are presented in Table 2.

The UV-absorption spectra of undoped and doped SnO_2 were carried out in a JASCO (Model V-670) UV–vis-NIR spectrophotometer in the wavelength range of 200–1000 nm for studying the band gap energy of the samples S1, S2, S3 and S4 sintered at 650 °C. The band gap energy values of different samples are calculated from the absorption edge corresponding to each sample by using the Tauc relation [28]:

$$\alpha h\nu = A(h\nu - E_g)^n$$

where α is the absorption coefficient, A is a constant, $n = 1/2$ for direct allowed transition, $h\nu$ is the photon energy taken from the UV-spectra and E_g is the optical band gap which could be calculated from $(\alpha h\nu)^2$ versus $(h\nu)$ plot as shown in Fig. 5. By extrapolating the linear part of the plot to $\alpha = 0$, the optical band gap of 4.1 eV was estimated for undoped SnO_2, while the optical band gap decreases with respective doping of Ni (3.95 eV), Ce (3.66 eV), and simultaneous Ni with Ce (3.58 eV) in SnO_2. The doping of Ni, Ce, and Ni with Ce in SnO_2 resulted into the decrease in band gap which reflected as red shift in absorption spectra [29–31] to a certain minimum value (i.e. critical size). The observed shift in band-gap values with dopants may be attributed to the change in energy eigen values as a result of perturbation potential due to exchange interaction.

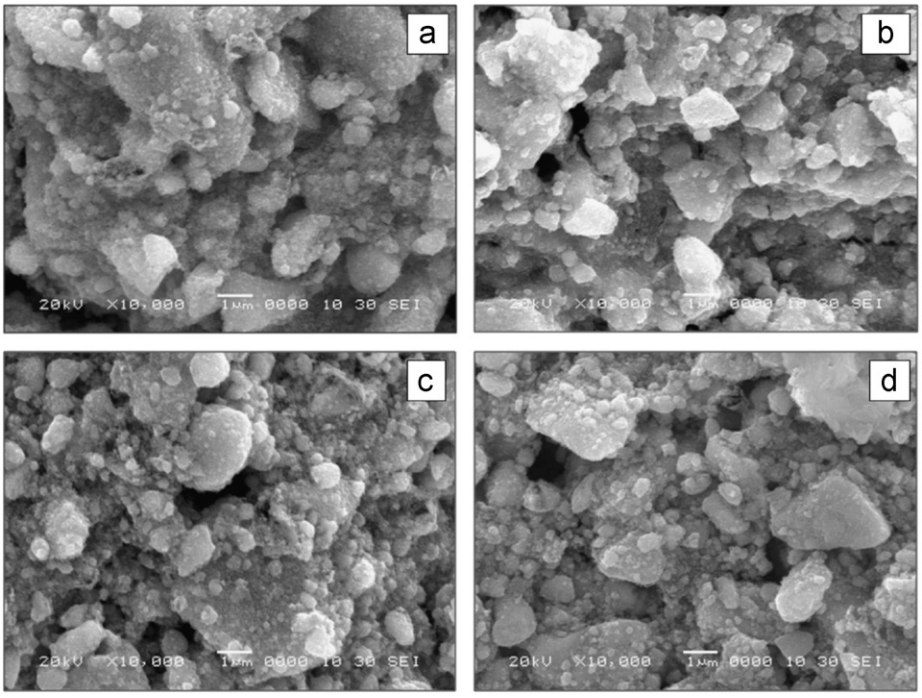

Fig. 2. SEM images of the surface of SnO_2 thick films: (a) undoped SnO_2 (b) Ni-doped SnO_2 (c) Ce-doped SnO_2 (d) (Ni+Ce)-doped SnO_2.

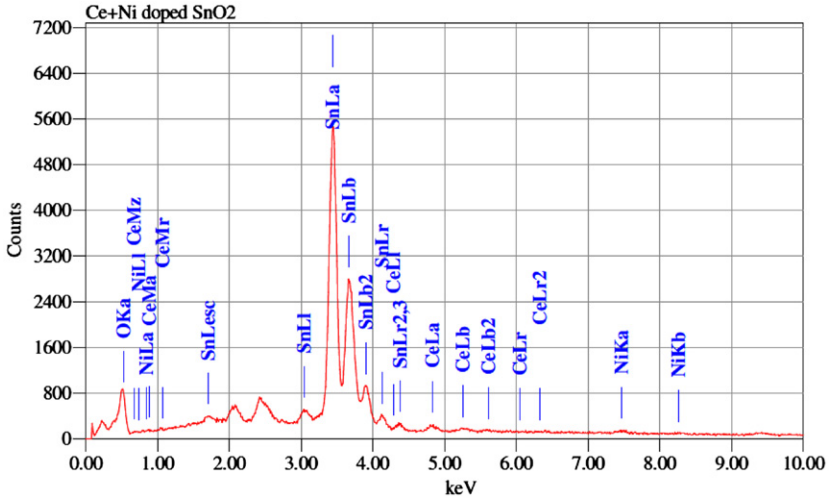

Fig. 3. EDAX spectrum of (Ni+Ce)-doped SnO_2 thick film.

Table 3
Element concentrations calculated from Energy Dispersive X-ray spectroscopy (EDAX) of (Ni+Ce)-doped SnO_2.

Element	Wt%	At%
Ce	2.62	0.89
Ni	0.84	0.68
Sn	73.55	29.65
O	23.00	68.77

FTIR analysis was carried out using a JASCO (Model Name FT/IR-6100 type A) spectrometer in the wavenumber range of 400–4000 cm^{-1} for studying the chemical groups on the surface of the samples S1, S2, S3 and S4 sintered at 650 °C. The detailed FTIR spectra of these samples are shown in Fig. 6. The peaks at 3500 cm^{-1} to 2500 cm^{-1} indicate presence of hydrogen bonds involved in O–H oscillators, which may be due to adsorbed water and Sn–OH groups. The peak which appeared at 573 cm^{-1} relates to the terminal oxygen vibration of Sn–OH, while the peak appearing at 652 cm^{-1} is due to the O–Sn–O bridge functional group of SnO_2 (S1). From Fig. 6 it is evident that with doping of Ni and Ce the position of characteristic vibration peaks of the Sn–OH and O–Sn–O functional groups in SnO_2 shifts towards higher wave number with maximum shift in case of S4, which is in agreement with the results reported earlier [32]. The shift in position of peaks is due to doping,

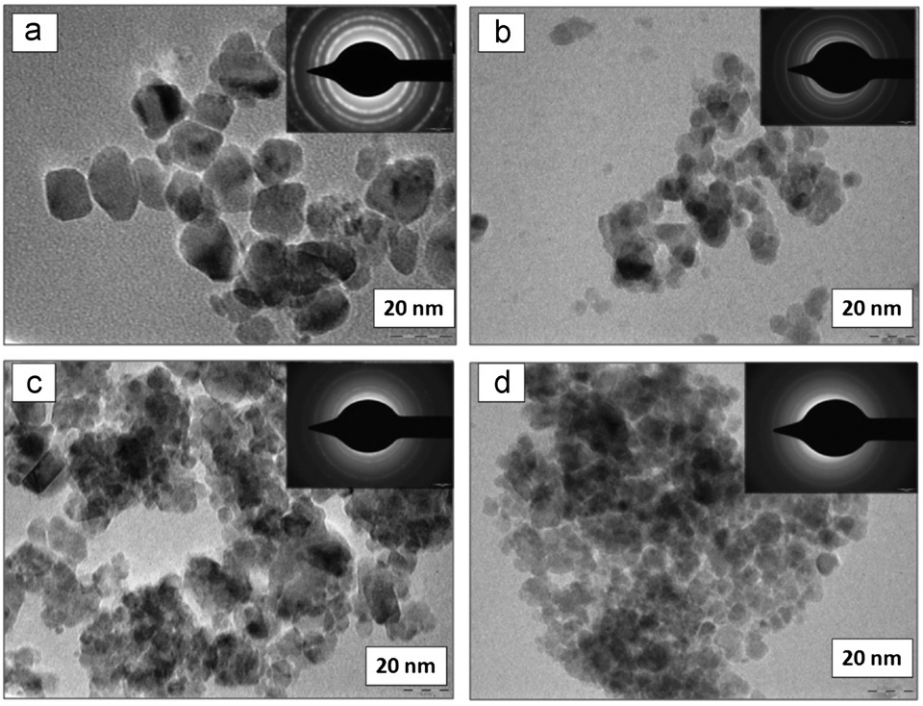

Fig. 4. TEM images with SAED patterns of SnO_2 thick films: (a) undoped SnO_2 (b) Ni-doped SnO_2 (c) Ce-doped SnO_2 (d) (Ni+Ce)-doped SnO_2.

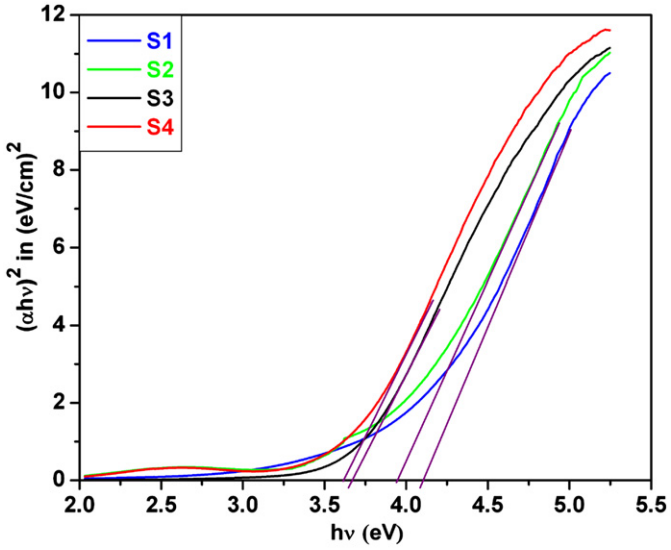

Fig. 5. UV spectra of undoped, Ni, Ce and (Ni+Ce)-doped SnO_2.

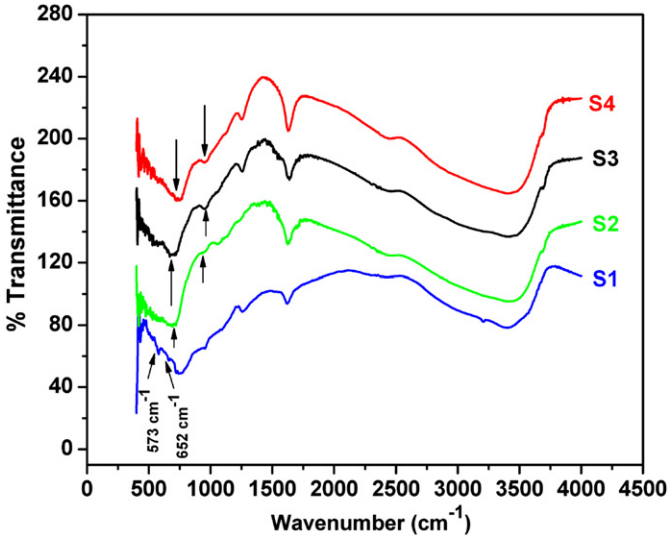

Fig. 6. FTIR spectra of undoped, Ni, Ce and (Ni+Ce)-doped SnO_2.

which reveals the formation of metastable solid solution, inhibiting the growth of nanoparticles [33,34].

3.2. Gas sensing properties

3.2.1. Gas response tests

We have examined the response of samples S1, S2, S3 and S4 towards acetone at 500 ppm concentration at various operating temperatures. The response and operating temperature were influenced by doping of Ni, Ce and Ni with Ce. In the present case we have observed increase in response and decrease in operating temperature with doping. The sample S1 exhibited response of 31%, while (Ni+Ce)-doped (S4) sample exhibited maximum response of 92% at 300 °C as shown in Fig. 7. The NiO and ceria might be acting as catalyst for the dissociation of acetone and are responsible for sensing it at relatively lower temperature.

The response of sintered thick films of S1, S2, S3 and S4 towards various test gases at 100 ppm was studied at an

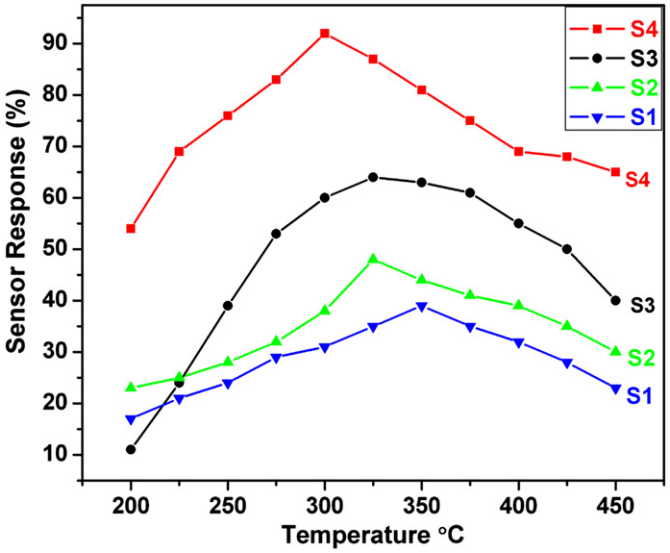

Fig. 7. Variation in sensor response towards fixed concentration (500 ppm) of acetone vapor measured at different temperature.

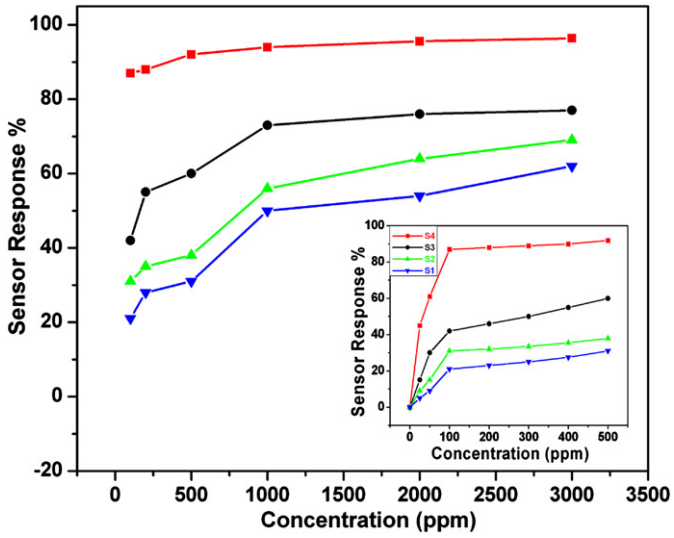

Fig. 9. Variation in sensor response to different concentrations of acetone vapor measured at 300 °C.

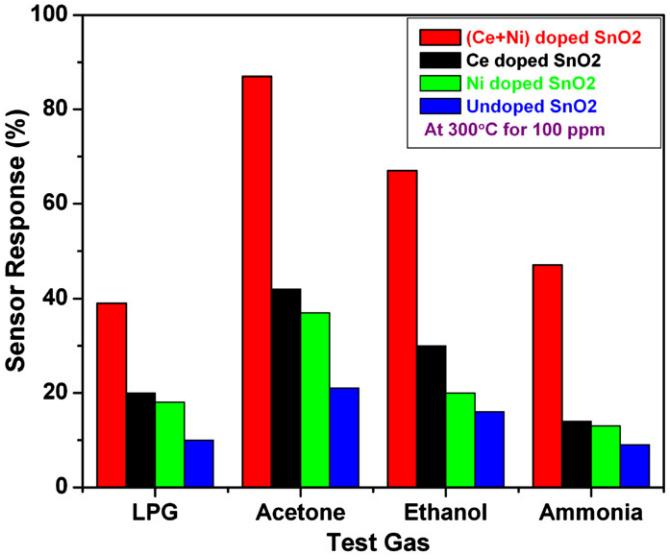

Fig. 8. Response (%S) for various gases for undoped and doped SnO_2 at 300 °C for 100 ppm concentration of gases.

optimum temperature of 300 °C. It can be seen from Fig. 8 that all the samples show high response and selectivity towards acetone in comparison with the other gases like LPG, ethanol and ammonia. It is found that for sample S4 the response is about 87% to 100 ppm acetone which is four times larger than that of S1 (21%). Thus S4 sample has proved to be the potential candidate for acetone detection at low concentration and relatively moderate operating temperature.

Fig. 9 shows the relation between response (%S) and concentration of acetone at 300 °C for undoped and doped SnO_2. It illustrates that the gas response increases with increase in concentration of acetone. Beyond 500 ppm the response of the S4 is found to be saturated, however the saturation limit in case of other samples (S1, S2 and S3) is at 1000 ppm. The inset in Fig. 9 shows the response as a function of concentration in the range 0–500 ppm of acetone. It reveals that from 0–200 ppm, the response increases linearly for all samples. Above 200 ppm, the response increases slowly up to 500 ppm; thereafter the sensor becomes more or less saturated.

In fact, the response (S) of a semiconductor metal oxide is usually represented by an empirical relation $S=A[C]^N+B$, where A and B are constants and C is the concentration of the target gas or vapor. N usually has a value between 0.5 and 1.0, depending on the change of the surface species and the stoichiometry of the elementary reactions on the surface [35]. As shown in the inset of Fig. 9, a curvilinear relationship between response and the acetone concentration has been observed, indicating $N=0.5$ for all samples. The slope of the sample S4 is greater than other samples which further confirm that the Ni with Ce-doped SnO_2 nanomaterial can be used as a promising material for acetone sensor.

The gas sensing mechanism of undoped and doped SnO_2 based sensor is the surface controlled process wherein resistance change is controlled by the species and amount of chemisorbed oxygen ions on the surface. Generally SnO_2 is known to exist in the non-stoichiometric form. It exists as $Sn(IV)_{1-x}\,Sn(II)_xO_{2-\delta}$ and the major impurity in SnO_2 is due to traces of Sn^{2+} and Sn^0 metallic. This is the reason why SnO_2 is generally nonstoichiometric with oxygen vacancy. When we dope Ni^{2+} and Ce^{3+} the overall effect cannot be called as p-type donor impurity. Thus it is observed that with incorporation of nickel and cerium in SnO_2, there is increase in potential barrier (resistance) without disturbing the overall n-type nature of SnO_2. The substitution of Sn^{4+} ions by lower valence Ni^{2+} and Ce^{3+} ions create more oxygen vacancies in the

sensor material and the presence of oxygen vacancies favors the adsorption of oxygen at optimized operating temperature improving the gas response of the material.

When atmospheric oxygen is adsorbed on the sensor surface, at high temperature, it traps the electrons from the conduction band of sensor material to produce negatively charged chemisorbed oxygen such as O^-; O_2^- and O^{2-}.

The reactions may proceed as follows: [cb: conduction band, ads: adsorbed]

$$O_{2(atm)} + e^-_{(cb)} \leftrightarrow O^-_{2(ads)}$$
$$O^-_{2(ads)} + e^-_{(cb)} \leftrightarrow 2O^-_{(ads)}$$
$$2O^-_{(ads)} + 2e^-_{(cb)} \leftrightarrow 2O^{2-}_{(ads)}$$

Thus the concentration of the electrons in the conduction band of SnO_2 decreases and hence the resistance of the material increases in air atmosphere. When Ni with Ce-doped SnO_2 sensor material is exposed to reducing gas (acetone), its resistance reduces in accordance with the well documented phenomenon of oxidation of reducing gas due to adsorbed oxygen ion species present on sensor. Hence the normal behavior of n-type material is observed which consequently reduces the potential barrier height. The maximum response of Ni with Ce-doped SnO_2 sensor towards acetone is probably due to smaller grain size which provides a large specific surface area and a higher surface activity, resulting into stronger interaction between acetone molecules and the adsorbed oxygen species. The overall reactions can take place as follows:

$$(CH_3)_2CO_{(gas)} + 4O^-_{2(ads)} \rightarrow 3CO_{2(gas)} + 3H_2O_{(gas)} + 4e^-_{(cb)}$$
$$NiO \rightarrow Ni^{2+} + 2e^-_{(cb)} + \tfrac{1}{2}O_2$$
$$2Ce_2O_3 \rightarrow 4Ce^{3+} + 12e^-_{cb} + 3O_2$$

The prominent role of ceria has been recognized in three way catalysis (TWC). The three-way catalyst is designed to simultaneously convert automobile exhaust pollutants (uncombusted hydrocarbons (HC), carbon monoxide (CO) and nitrogen oxides (NO_x)) to environmentally acceptable products such as carbon dioxide, water and nitrogen. It is well known from electronic structure calculations of cerium oxide (ceria) that it has two forms viz. CeO_2 (cubic fluorite in structure) and Ce_2O_3 (hexagonal lattice in structure). Ceria is widely applied in automobile exhaust catalysts as an oxygen storage, due to its stability to take and release oxygen under oxidizing and reducing conditions. This is due to continuous ongoing transformation between the two Ce oxides, the oxygen-rich CeO_2 and the oxygen-poor Ce_2O_3 depending on the external oxygen concentration.

In the presence of acetone, the Ce_2O_3 is converted into Ce [36,37]:

$$Ce_2O_3 + CH_3COCH_3 \rightarrow Ce + C_2H_4 + H_2O + CO_2$$

In the absence of acetone, Ce gets quickly oxidized to Ce_2O_3:

$$4Ce + 3O_2 \rightarrow 2Ce_2O_3$$

Fig. 10 shows variation of ln R versus $1000/T$ in air for different samples. The electrical resistance increased with nickel doping and it was further enhanced with nickel and cerium doping. The increasing trend may be due to the increase in the depletion layer thickness. As Ni^{2+} and Ce^{3+} replaces some of Sn^{4+} ions, so there is net decrease in the charge carrier concentration which results in increase in barrier height at the grain boundaries. From Arrhenius plot the activation energy was calculated. The activation energy values are found to increase with doping of nickel (0.90 eV), cerium (0.98 eV) and nickel-cerium (1.21 eV) as compared to undoped SnO_2 sample (0.81 eV). The activation energy may not be always equal to barrier height, particularly in oxides. We assume that the increase in activation energy is due to formation of deep defect

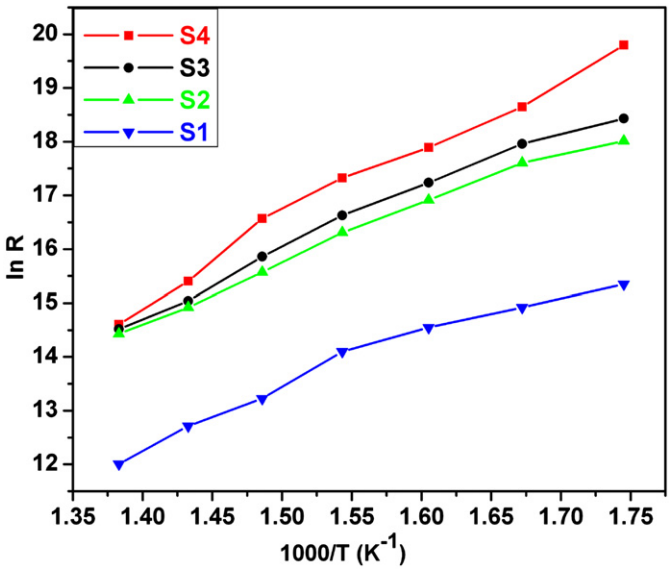

Fig. 10. Variation of ln R with $1000/T$ (K^{-1}).

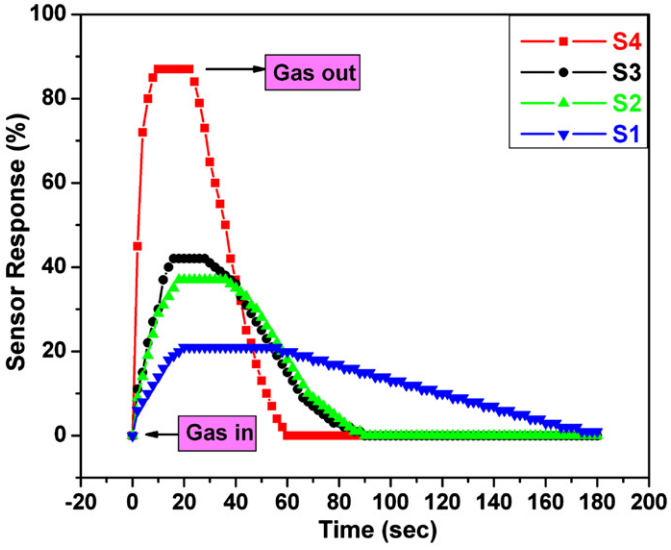

Fig. 11. Transient response characteristics of undoped and doped SnO_2 exposed to 100 ppm acetone vapor at 300 °C.

Table 4
Response and recovery characteristics for 100 ppm of acetone vapor at operating temperature of 300 °C.

Time	Undoped SnO_2 (S1)	Ni-doped SnO_2 (S2)	Ce-doped SnO_2 (S3)	(Ni + Ce)-doped SnO_2 (S4)
$t_{response}$	55 s	35 s	28 s	23 s
$t_{recovery}$	3 min	1.5 min	1.5 min	1 min

states, which may be interstitials. Due to the formation of more defect states they create separate band in the energy band diagram and lower the band gap which in turn reduces the barrier height too, we mean 'band tailing' effect.

The transient response characteristics of all the samples exposed to 100 ppm acetone concentration at an operating temperature of 300 °C are shown in Fig. 11. In these measurements, sensors response as a function of time was measured. From figure it is obvious that, as we go from S1 to S4 the sensor response is found to enhance significantly, which is attributed to the change in morphology and reduction in crystallite size of the sample with doping, which facilitates the adsorption of oxygen significantly. In case of S4, the number of active adsorption sites for oxygen is high as compared to S1, S2 and S3. The adsorption of oxygen on the surface increases the resistance of the sensor material due to transport of electrons from conduction band to adsorbed oxygen which results in increase in gas response.

3.2.2. Response and recovery time

Table 4 reveals that with doping Ni and Ce promotes the gas response; the response and recovery characteristics for S4 at 300 °C shows that for 100 ppm of acetone the resistance drops within 23 s and regains the original value within 1 min. The doping of Ni and Ce improves the gas response and recovery time as compared with other samples (S1, S2 and S3). Such an increase in the selective response towards acetone with fast response and recovery time is attributed to simultaneous doping of Ni and Ce. The faster response and recovery may be due to the high reactivity of acetone vapor with adsorbed oxygen in the presence of Ni and Ce sites on the surface of the sensor. The faster response and recovery would also be attributed to the highly porous nature of the sensor. Fast and easier gas diffusion to grain boundaries would enable the gas to be oxidized immediately, giving faster response.

4. Conclusions

Undoped, nickel, cerium, and nickel with cerium doped nanocrystalline tin oxide powders were successfully synthesized by co-precipitation route. The incorporation of Ni, Ce and Ni with Ce is found to introduce significant structural and morphological changes in SnO_2. The reduction in grain size is due to incorporation of these metal oxides which favors the interaction between the material surface and the test gas. The sensor S4 (Ni with Ce-doped SnO_2) exhibited selective acetone response with rapid response (23 s) and fast recovery (~1 min) at 100 ppm. The simultaneous doping of Ni and Ce in SnO_2 showed profound effect on the gas sensing properties hence it can be used as promising candidate for the fabrication of high-performance acetone gas sensor.

Acknowledgments

One of the authors, Latika K. Bagal would like to thank the University Grants Commision (UGC) for providing teacher fellowship under FIP and Dr. K. N. Ganage, Principal, K.B.P.M. Pandharpur. J.Y. Patil acknowledges DAE-BRNS for the grant of JRF. I.S. Mulla is grateful to CSIR, India for granting Emeritus Scientist Fellowship. All the authors gratefully acknowledge DAE-BRNS, India for the financial support. Authors kindly acknowledge the SAIF—IIT Bombay for providing the TEM facility.

References

[1] S.S. Likhodii, K. Musa, S.C. Cunnane, Breath acetone as a measure of systemic ketosis assessed in a rat model of the ketogenic die, Clinical Chemistry 48 (2002) 115–120.
[2] N. Makisimovich, V. Vorotyntsev, N. Nikitina, O. Kaskevich, P. Karabun, F. Martynenko, Adsorption semiconductor sensor for diabetic ketoacidosis diagnosis, Sensors and Actuators B 36 (1996) 419–421.
[3] C.H. Deng, J. Zhang, X.F. Yu, W. Zhang, X.M. Zhang, Determination of acetone in human breath by gas chromatography–mass spectrometry and solid-phasemicroextraction with on-fiber derivatization, Journal of Chromatography B 810 (2004) 269–275.
[4] C.H. Deng, W. Zhang, J. Zhang, X.M. Zhang, Rapid determination of acetone in human plasma by gas chromatography–mass spectrometry and solid-phasemicroextraction with on-fiber derivatization, Journal of Chromatography B 805 (2004) 235–240.
[5] N.D. Totir, S. Velea, C. Lete, C. Neamtu, Pinacol synthesis by acetone reduction coupling, Revue de Chimie 48 (1997) 489–493.
[6] J.G. Duh, J.W. Jou, B.S. Choi, Catalytic and gas sensing characteristics in Pd doped SnO_2, Journal of The Electrochemical Society 136 (1989) 2740–2747.
[7] A.R. Phani, S. Manorama, V.J. Rao, Effects of additives on the response of sensors utilizing semiconducting oxide on carbon monoxide sensitivity, Applied Physics Letters 66 (25) (1995) 3489–3491.
[8] D.S. Vlachos, C.A. Papadopoulos, J.N. Avarisiotis, On the electronic interaction between additives and semiconducting oxide gas sensors, Applied Physics Letters 69 (1996) 650–652.
[9] M. Fleischer, S. Kornely, T. Weh, J. Frank, H. Meixner, Selective gas detection with high temperature operated metal oxides using catalytic filters, Sensors and Actuators B 69 (2000) 205–210.
[10] C. Xu, J. Tamaki, N. Miura, N. Yamazoe, Promotion of tin oxide gas sensor by aluminium doping, Talanta 38 (10) (1991) 1169–1175.
[11] R. Rai, Study of structural and electrical properties of pure and Zn–Cu doped SnO_2, Advanced Materials Letters 1 (1) (2010) 55–58.

[12] K. Jain, R.P. Pant, S.T. Lakshmikumar, Effect of Ni doping on thick film SnO_2 gas sensor, Sensors and Actuators B 113 (2006) 823–829.
[13] S.B. Patil, P.P. Patil, M.A. More, Acetone vapour sensing characteristics of cobalt doped SnO_2 thin films, Sensors and Actuators B 125 (2007) 126–130.
[14] M. Peiteado, Y. Iglesias, J. De Frutos, J.F. Fernandez, A.C. Caballero, Preparation of ZnO–SnO_2 ceramic materials by a coprecipitation method, Boletin de la Sociedad Espanola de Ceramica y vidrio 45 (3) (2006) 158–162.
[15] J.H. Yu, G.M. Choi, Selective CO gas detection of CuO- and ZnO-doped SnO_2 gas sensor, Sensors and Actuators B 75 (2001) 56–61.
[16] K. Gopinadhan, S.C. Kashyap, D.K. Pandya, S. Chaudhary, High temperature ferromagnetism in Mn-doped SnO_2 nanocrystalline thin films, Journal of Applied Physics 102 (2007) 11 (art. no. 113513).
[17] F.H. Aragon, J.A.H. Coaquira, P. Hidalgo, S.W. da Silva, S.L.M. Brito, D. Gouvea, P.C. Morais, Evidences of the evolution from solid solution to surface segregation in Ni- doped SnO_2 nanoparticles using Raman spectroscopy, Journal of Raman Spectroscopy 42 (5) (2011) 1081–1086.
[18] R.S. Niranjan, K.R. Patil, S.R. Sainkar, I.S. Mulla, High H_2S-sensitive copper-doped tin oxide thin film, Materials Chemistry and Physics 80 (2003) 250–256.
[19] A. Mosquera, J.E. Rodringuez-Paez, J.A. Varela, P.R. Bueno, Synthesis of SnO_2 by chemical routes and its use in varistor production, Journal of the European Ceramic Society 27 (2007) 3893–3896.
[20] A.D. Garje, R.C. Aiyer, Effect of decomposition temperature on electrical and gas sensing properties of nano SnO_2 based thick film resistors, Sensor Letters 4 (2006) 380–387.
[21] A. Chiorino, G. Ghiotti, F. Prinetto, M.C. Carrota, Preparation and characterization of SnO_2 and WOx–SnO_2 nanosized powders and thick films for gas sensing, Sensors and Actuators B 78 (2001) 89–97.
[22] R.C. Pawar, J.S. Shaikh, A.V. Moholkar, S.M. Pawar, J.H. Kim, J.Y. Patil, S.S. Suryavanshi, P.S. Patil, Surfactant assisted low temperature synthesis of nanocrystalline ZnO and its gas sensing properties, Sensors and Actuators B 151 (2010) 212–218.
[23] R.D. Shannon, Revised effective ionic radii and systemetic studies of interatomic distancesin halides and chalcogenides, Acta Crystallographica A 32 (1976) 751–767.
[24] C. Li, Z. Yu, S. Fang, S. Wu, Y. Gui, R. Chen, Synthesis and gas sensing properties of Ce-doped SnO_2 materials, Journal of Physics: Conference Series 152 (2009) 012033.
[25] G. Korotcencov., V. Brinzari., I. Boris, (Cu, Fe, Co or Ni)-doped tin dioxide films deposited by spray pyrolysis: doping influence on film morphology, Journal of Materials Science 43 (8) (2008) 2761–2770.
[26] F. Pourfayaz, A. Khodadadi, Y. Mortazavi, S.S. Mohajerzadeh, CeO_2 doped SnO_2 sensor selective to ethanol in presence of CO, LPG and CH_4, Sensors and Actuators B 108 (2005) 172–176.
[27] A.B. Gambhire, M.K. Lande, S.B. Kalokhe, M.D. Shirsat, K.R. Patil, R.S. Gholap, Synthesis and characterization of high surface area CeO_2-doped SnO_2 nano material, Materials Chemistry and Physics 112 (2008) 719–722.
[28] J.I. Pankove, Optical Process in Semiconductors, New Jersey USA 34 1971, p. 93.
[29] H. Lin, C.P. Huang, W. Li, C. Ni, S.Ismat Shah, Yao-Hsuan Tseng, Size dependency of nanocrystalline TiO_2 on its optical property and photocatalytic reactivity exemplified by 2-chlorophenol, Applied Catalysis B: Environmental 68 (2006) 1–11.
[30] R.N. Mariammal, N. Rajamanickam, K. Ramachandran, Synthesis and characterization of undoped and Co-doped SnO_2 nanoparticles, Journal of Nano- and Electronic Physics 1 (3) (2011) 92–100.
[31] P. Silija, Z. Yaakob, V. Suraja, N.N. Binitha, Z.S. Akmal, An enthusiastic glance in to the visible responsive photocatalysts for energy production and pollutant removal, with special emphasis on titania, review article, International Journal of Photoenergy 2012 (2012) (Article ID 503839, 19 pages).
[32] J. Zhang, L. Gao, Study of electrical properties of nickel doped SnO_2 ceramic nanoparticles, Solid State Chemistry 177 (2004) 1425–1430.
[33] N. Sergent, P. Gelin, L. Perier-Camby, H. Praliaud, G. Thomas, Preparation and characterisation of high surface area stannic oxides: structural, textural and semiconducting properties, Sensors and Actuators B 84 (2002) 176–188.
[34] G. Brankovic, Z. Brankovik, M.R. Davolos, M. Cilense, J.A. Varela, Influence of the common varistor dopants (CoO, Cr_2O_3 and Nb_2O_5) on the structural properties of SnO_2 ceramics, Materials Characterization 52 (2004) 243–251.
[35] Z. Wang, L. Liu, Synthesis and ethanol sensing properties of Fe-doped SnO_2 nanofibers, Materials Letters 63 (2009) 917–919.
[36] Irie Shinji, Okita Hironobu, Mizushima Takanori, Kakuta Noriyoshi, Reduction behavior of CeO_2 dispersed on ZrO_2, Journal of Rare Earths 44 (2004) 188–189.
[37] C. Li, K. Domen, K.I. Maruya, T. Onishi, Complete oxidation of carbon monoxide and methane over metal-promoted fluorite oxide catalysts, Journal of the American Chemical Society 111 (1989) 7683–7687.